Instabilities Across the Isotropic Conductivity Point in a Nematic Phenyl Benzoate under AC Driving

ARTICLE *in* THE JOURNAL OF PHYSICAL CHEMISTRY B · SEPTEMBER 2007

Impact Factor: 3.3 · DOI: 10.1021/jp072686o · Source: PubMed

4 AUTHORS:

Pramoda Kumar
Harvard University
15 PUBLICATIONS **122** CITATIONS
SEE PROFILE

Shivaram N. Patil
Karnatak University, Dharwad
6 PUBLICATIONS **14** CITATIONS
SEE PROFILE

Uma Hiremath
Centre for Nano and Soft Matter Sciences
52 PUBLICATIONS **597** CITATIONS
SEE PROFILE

K. S. - Krishnamurthy
Centre for Nano and Soft Matter Sciences (fo…
41 PUBLICATIONS **239** CITATIONS
SEE PROFILE

Instabilities Across the Isotropic Conductivity Point in a Nematic Phenyl Benzoate under AC Driving

Pramoda Kumar,[†] Shivaram N. Patil,[‡] Uma S. Hiremath,[†] and K. S. Krishnamurthy*[,†]

Centre for Liquid Crystal Research, P. O. Box 1329, Jalahalli, Bangalore 560 013, India, and Garden City College, Virgonagar Post, Bangalore 560 049, India

Received: April 5, 2007; In Final Form: May 14, 2007

We characterize the sequence of bifurcations generated by ac fields in a nematic layer held between unidirectionally rubbed ITO electrodes. The material, which possesses a negative dielectric anisotropy ϵ_a and an inversion temperature for electrical conductivity anisotropy σ_a, exhibits a monostable tilted alignment near T_{IN}, the isotropic−nematic point. On cooling, an anchoring transition to the homeotropic configuration occurs close to the underlying smectic phase. The field experiments are performed for (i) negative σ_a and homeotropic alignment, and (ii) weakly positive σ_a and nearly homeotropic alignment. Under ac driving, the Freedericksz transition is followed by bifurcation into various patterned states. Among them are the striped states that seem to belong to the dielectric regime and localized hybrid instabilities. Very significantly, the patterned instabilities are not excited by dc fields, indicating their possible gradient flexoelectric origin. The Carr−Helfrich mechanism-based theories that take account of flexoelectric terms can explain the observed electroconvective effects only in part.

Introduction

The response of a nematic fluid to an external electric field is determined by several factors relating to material and field parameters, and the sample configuration. Much of the vast literature devoted to electrically driven instabilities in nematics dwells on one or the other of two different phenomena: First, purely orientational equilibrium effects such as caused by dielectric anisotropy, flexoelectric polarization and surface polarization; second, nonequilibrium dissipative effects, as found in the vortical flows attributable to anisotropic electrical conduction, charge injection at the electrodes or surface charge inhomogeneity.[1−4] Situations involving interplay of different bifurcation mechanisms are of particular relevance to nonlinear science and, in recent years, a few significant studies have been conducted in this area. For instance, Delev et al.[5] have reported their experimental and theoretical results concerning the crossover between flexoelectric and electroconvective distortions occurring in a homeoplanar nematic subject to a dc field. Similarly, Dressel et al.[6] have demonstrated the coupling of homogeneous and vortex modes to generate the so-called splay and twist normal rolls. More recently, Dressel and Pesch[7] have reported their rigorous theoretical analysis of the competition between electroconvection (EC) and the Freedericksz effect (FE), and we have discussed the experimental results relating to this competition.[8] In this paper, we report mainly on some hybrid electroconvective instabilities arising within the Freedericksz distorted state of a nematic.

Nematic EC due to anisotropic material parameters is principally governed by $\epsilon_a = (\epsilon_{||} - \epsilon_\perp)$ and $\sigma_a = (\sigma_{||} - \sigma_\perp)$, || and ⊥ denoting the directions relative to the nematic director **n**. Nematics with negative ϵ_a, positive σ_a, and planar alignment p, conveniently referred to as (− + p) compounds, taken between ITO-coated glass plates and driven by a field along the substrate normal, are established as the ideal candidates to exhibit a well ordered sequence of hydrodynamic instabilities, starting with periodic rolls at a threshold voltage and developing into chaotic flows far from equilibrium.[9] These classic instabilities are understood essentially on the basis of the so-called Carr−Helfrich (CH) mechanism that addresses, for the applied dc field, the coupling between σ_a and the bend curvature distortion leading to periodic space charges of alternating sign along the initial director. The body force due to these charges sets up periodic cellular flows above a voltage threshold V_c, which, in turn, is determined by the balance between the destabilizing hydrodynamic and transverse-field torques, and the stabilizing dielectric and elastic torques. The corresponding one-dimensional (1-D) analysis for an ac field of frequency ω predicts[10] the instability threshold field $E_c(\omega)$ to be

$$E_c^2(\omega) = \frac{\epsilon_{||} k_{33} \lambda^2 (1 + \omega^2\tau^2)}{\epsilon_o \epsilon_a \epsilon_\perp (1 + \omega^2\tau^2 - \zeta^2)}; \qquad \zeta^2 = \left(1 - \frac{\sigma_\perp \epsilon_{||}}{\sigma_{||} \epsilon_\perp}\right)\left(1 + \frac{\epsilon_{||}}{\epsilon_a}\frac{\alpha_2}{\eta_1}\right); \qquad \tau = \frac{\epsilon_o \epsilon_{||}}{\sigma_{||}} \quad (1)$$

where k_{33} denotes the bend elastic constant, λ the period of stripes, τ the charge relaxation time, and ζ^2 the Helfrich parameter; α_2 and η_1 are the Leslie and Miesowicz viscosity coefficients, respectively. The cutoff frequency $\omega_c = \sqrt{(\zeta^2 - 1)/\tau}$ defines the limit of the conduction regime within which the space charges oscillate at the field frequency while the director pattern is static. Beyond ω_c, in the dielectric regime, the space charges are static, but the director oscillates. The occurrence of instability in either regime requires $(\zeta^2 - 1)$ to be positive.

Goscianski and Leger[11] were perhaps the first to consider the effect of varying $(\zeta^2 - 1)$ between positive and negative values via temperature dependent σ_a in nematics with an

* Corresponding author. E-mail: murthyksk@gmail.com.
† Centre for Liquid Crystal Research.
‡ Garden City College.

10.1021/jp072686o CCC: $37.00
Published on Web 07/06/2007

underlying smectic phase. They did observe convective instabilities for $\xi^2 < 1$ corresponding to the (− − p) case of 4-*n*-butoxybenzylidene-4′-octylaniline (**4O.8**) and di-*n*-4-4′-octyloxyazoxybenzene (**C8**). The corresponding low-frequency pattern consists of zigzag domains predominantly directed along **n,** rather than normal to **n** as in the classic Williams roll pattern,[1] and is conjectured to arise from an amplification of twist fluctuations caused by the Leslie coefficient α_3 being positive. Subsequently, Tikhomirova et al.[12] reported for (**4O.7**) in the (− − p) configuration, a threshold pattern of "longitudinal domains", parallel to **n** and involving both polar (θ) and azimuthal (φ) angular deviations of the director. They interpreted it as either due to the CH effect appropriate to the (− − t) configuration, *t* signifying an initial director tilt, or due to a two-dimensional flexoelectric instability. Blinov et al.[13] later confirmed the occurrence of longitudinal domains in (**4O.4**), (**4O.7**), and (**4O.8**) in the (− − p) case; and also observed a fingerprint texture in the (+ − h) case, h denoting the homeotropic director pattern. They ascribed the instabilities qualitatively to a combination of isotropic and CH mechanisms. Petrov and Simova[14] also reported temperature-dependent electroconvective pattern changes for 4-*n*-hexyloxyphenyl-4′-*n*-decyloxybenzoate (**10**/**6**), homogeneously aligned in the field-off state. Their observations seem to indicate a tilted to planar transition taking place while heating, although no assertion of this is made by them. Further, their high temperature Williams-like rolls, in the light of later developments, seem to correspond to the (− + p) case while the longitudinal domains formed well below the N−I point may represent the (− − t) case.

Recently, Kochowska et al.[15] have examined in detail electroconvection for the (− − p) case in **10**/**6**, exhibiting a temperature induced sign inversion of σ_a. They observe electroconvective structures with similar morphological features as in other nematics exhibiting σ_a inversion[11−14] and categorize them under nonstandard electroconvection (NSEC) in view of their nonconformity to the so-called standard model (SM), which is a three-dimensional generalization of the earlier CH-mechanism-based theories.[3,16] In a report due to be published, Katona et al.[17] have further observed NSEC with Hopf bifurcation in **8**/**7** studied in the (− − p) configuration. Buka et al.[18] have reviewed recently the various possible pattern-forming instabilities for the eight combinations between the signs of ϵ_a and σ_a, and the initial alignment (either p or h) with reference to the SM.

The foregoing survey of the earlier work shows that there has been no report of experimental investigations pertaining to the (− − h) case. While examining the thermal behavior of **10**/**5**, we noticed, as we approached the N−I transition from below, a temperature induced anchoring transition from the homeotropic to the tilted state. The sample also displayed σ_a sign inversion within the nematic range. We made use of these findings to carry out a detailed study of the electroconvective instabilities in the (− − h) and (− + t) cases and found several distinguishing textural features not encountered in previous studies on materials with σ_a inversion behavior. It is our main purpose here to characterize the sequence of bifurcations for the two cases mentioned, describe the novel features of NSEC that involve a coupling between different destabilization mechanisms, and discuss the significance of the patterned states.

Experimental Methods

The compound used is 4-*n*-pentyloxyphenyl 4-*n*-decyloxybenzoate (**10**/**5**):

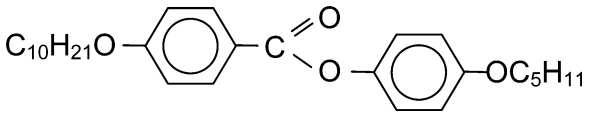

with the phase sequence:

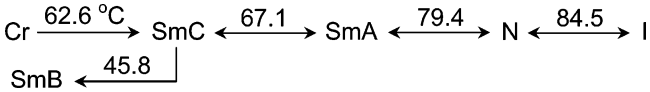

The sample cells were sandwich type, constructed of passivated, ITO-coated glass plates from Delta Technologies. The electrodes were used without any blocking layers, after rubbing unidirectionally with a tissue paper some 100 times. The rubbing direction and the layer normal define the reference axes *x* and *z*, respectively. Mylar spacers, heat-sealed to the electrodes through cooling from ∼250 °C under a uniform pressure, determined the cell spacing, *d*. The *d*-value, from cell capacitance measurements, was ∼30 μm. Observations were carried out in transmitted light along *z*, using a Leitz DMRXP polarizing microscope, equipped with a Mettler hot-stage. The images were recorded using a Sony CCD camera. The electric field was applied along *z*. The voltage source was a Stanford Research Systems DS 345 function generator coupled to a FLC Electronics voltage amplifier (Model A800). The applied voltage was measured with a HP 34401A multimeter. For dielectric and conductivity measurements, we employed an Agilent 4284A precision LCR meter.

For convenience, the polarizer with the transmission axis along *x* and the analyzer along *y*, will be represented as *P*(*x*)−*A*(*y*); *P*(45)−A(135) indicates diagonal setting of polarizer and analyzer, with the angles in degrees measured from the *x* direction in parentheses.

Results

A. Dielectric and Conductivity Anisotropies. Kresse et al.[19] have carried out detailed dielectric measurements on **10**/**5** employing a magnetic field of 0.5 T for sample alignment. Our independent measurements on static permittivity with an aligning field of 1.5 T (Figure 1a), agree with their data to within 10%. Figure 1b shows ϵ_a as a function of temperature. In Figure 2a we present our data on electrical conductivity along and perpendicular to the nematic director measured at different temperatures, and Figure 2b shows the corresponding temperature variation of σ_a. It is relevant to note that σ_a changes sign at ∼81.5 °C and this crossover is a pretransitional fluctuation effect arising due to the underlying smectic phase. Similar findings have been reported in ref 15 for the phenyl benzoates **10**/**6**, **10**/**4**, and **8**/**7**.

B. Anchoring Transition. With the aim of obtaining a planarly aligned nematic monodomain, we employed paper-buffed ITO plates for cell construction, as previously mentioned. The liquid sample drawn by capillarity into the cell kept initially at 110 °C was cooled very slowly at a programmed rate of 0.1 °C min^{-1} to a temperature slightly below T_{IN}. Then the alignment was uniform, but not planar. We found a tilted structure which on further cooling changed over to homeotropic orientation near the N−SmA transition temperature, T_{NA}. There occurred an anchoring transition at about 80.5 °C from a monostable tilted configuration with the C_1 symmetry to the homeotropic state with the C_∞ symmetry. We found this transition to be reversible without any significant hysteresis showing it to be continuous. The conoscopic images in Figure 3, obtained during heating from the lower limit of the N range,

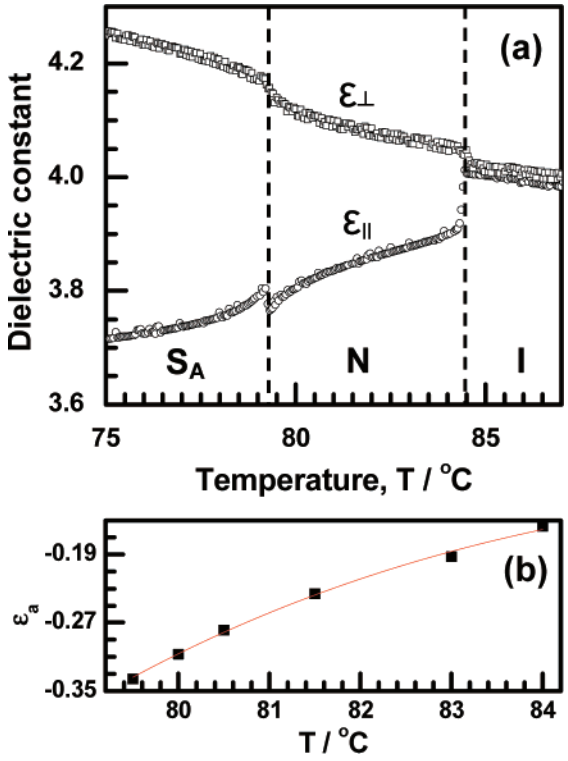

Figure 1. (a) Temperature variation of the dielectric constants $\epsilon_{||}$ and $\epsilon_{\perp}$ in **10**/**5** measured at 10 kHz using an aligning field of 1.5 T. (b) Dielectric anisotropy as a function of temperature.

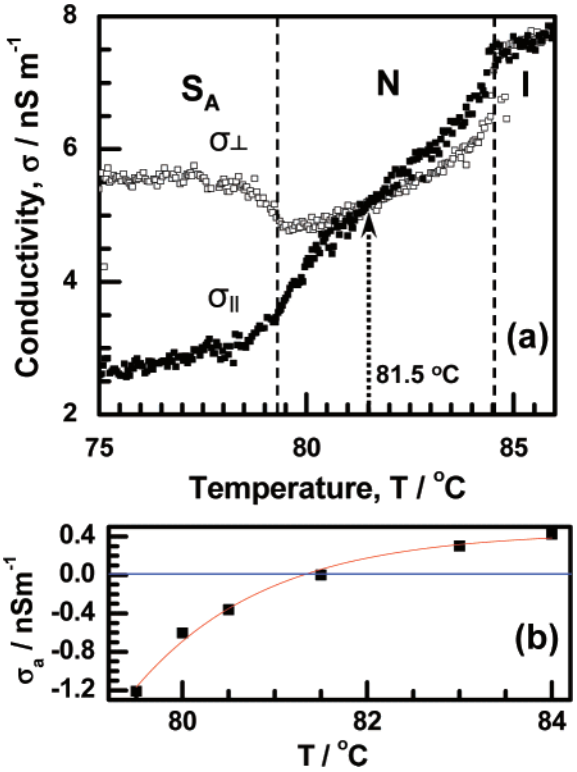

Figure 2. (a) Temperature variation of the electrical conductivities $\sigma_{||}$ and $\sigma_{\perp}$ in **10**/**5** measured at 10 kHz using an aligning field of 1.5 T. (b) Conductivity anisotropy as a function of temperature.

illustrate the nature of alignment at different temperatures. In Figure 3a, the Maltese cross is well centered and a definitive shift of the melatope to the left along *x*, the rubbing direction, is discernible in Figure 3c. The tilt of the optic axis θ from the layer normal *z* is approximately obtained from sin θ = (N.A./n_o) (R/R_o) where N.A. is the numerical aperture (=0.4), n_o the ordinary refractive index (~1.47), R the distance of the melatope from the center and R_o the radial dimension of the uniaxial cross; the tilt in Figure 3c is about 1.7° and in Figure 3d, 14°. A further increase in θ is indicated in Figure 3e, but a completely planar alignment is not obtained. It is interesting to note that the tilt change, which sets in at a temperature T_c of ~80.5 °C, is far less at T = 81.5 °C than at T = 82.5 °C, showing a rapid increase in θ over a narrow temperature range. This trend is reminiscent of the nature of continuous homeotropic-to-tilted nematic anchoring transition observed previously in the Merck racemic mixture "SCE12R", near T_{NA}, at a polyimide-coated and strongly rubbed substrate.[20a] This has been explained by the Landau model, considering two competing forces, one promoting the planar director field and the other the homeotropic field, and also the tilt elasticity due to the growth of surface-induced short-range smectic order. A related, much earlier report concerns the occurrence of sudden, hysteretic transition between the homeotropic and planar states close to T_{NA} in nematic **4O.8**;[20b] it has been attributed to the entropy change due to the smectic order at the substrates prevailing under weak anchoring conditions.

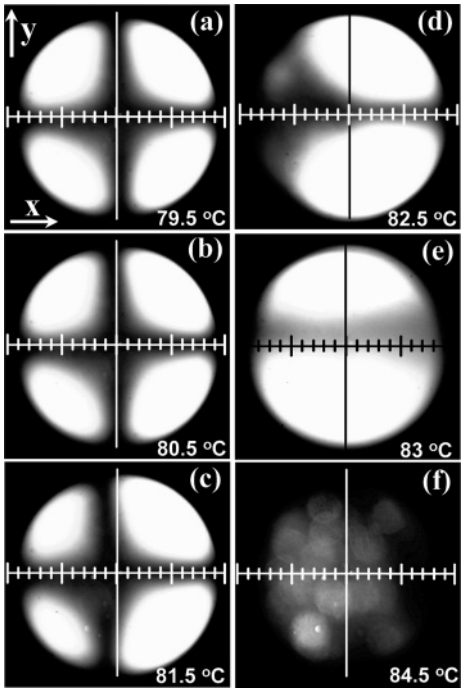

Figure 3. Interference figures under conoscopic examination between crossed polarizers $P(x)-A(y)$ corresponding to different temperature dependent orientations of the uniaxial structure. The figures are centered in panels a and b; the progressive and predominantly leftward shift of the melatope is evident in panels c−e. The sample is melting in panel f. The sequence is reversed on cooling. Each division on the horizontal scale is 10 μm.

C. Freedericksz Transition. Since ϵ_a is negative for **10**/**5**, both homeotropic and uniformly tilted samples experience the dielectric torque under the applied field, and above a temperature-dependent threshold V_F, determined by the balance between the elastic and dielectric torques, reorientation toward the planar state occurs. We determined V_F from the cell capacitance−voltage plots as illustrated in Figure 4. Slightly above the SmA−N transition temperature T_{AN}, the capacitance, which remained constant till V_F, increased sharply thereafter; near T_{NI}, on the other hand, there was a continuous increase in capacitance at a rate that changed discernibly at V_F. In fact, for a sample with a homogeneous oblique orientation in the field-

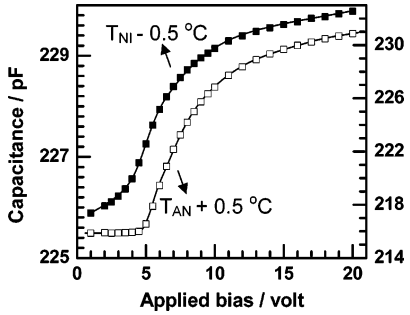

Figure 4. Cell capacitance close to the N−I (left ordinate) and SmA−N (right ordinate) transition points as a function of applied bias.

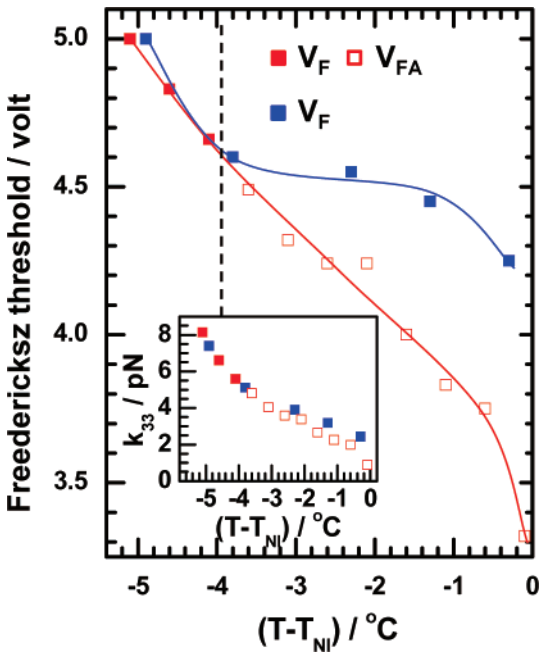

Figure 5. Dependence of Freedericksz threshold on temperature. The open and filled red squares are for the same sample exhibiting an anchoring transition at the temperature indicated by the vertical dashed line. The blue squares are for a homeotropic sample without any anchoring transition. V_F and V_{FA} denote, respectively, the actual and apparent Freedericksz thresholds. The inset shows the temperature variation of the bend elastic constant k_{33} for the two samples (see text).

off state, the initial tilt plays the role of an external field and the orientational distortion is finite at any finite applied field E, disappearing only for $E = 0$; although the phase transition is thus removed by the initial tilt, the field-induced tilt displays an apparent transition at $V \approx V_F$.[2] More specifically, if we denote the incremental director deviation $(\theta - \theta_o)$ by β, it can be shown that, as long as β is small, its maximum midplane value β_m is, under one elastic constant approximation, given by[21a]

$$\beta_m = \frac{\tan(2\theta_o)}{2}\left[\frac{1}{\cos\{(\pi V/2V_F)\sqrt{\cos(2\theta_o)}\}} - 1\right]$$

For applied bias below V_F, this expression simplifies to $\beta_m = \beta_{mF}(V/V_F)^2$ with $\beta_{mF} = (\pi^2/16)\sin(2\theta_o)$ signifying the β_m value for $V = V_F$. For voltages slightly above V_F, where β_m is relatively large, we have $\beta_m = \beta_{mF} + 2[(V - V_F)/V_F]^{1/2}$. Thus, $(d\beta_m/dV)$, or by implication the voltage rate of cell capacitance change, markedly rises beyond V_F, the apparent transition occurring at $V_{FA} < V_F$. In Figure 5, we present the temperature variation of the Freedericksz threshold whether real or apparent. The dependence of bend elastic constant k_{33} on temperature, derived from the data in Figures 1 and 5, by equating V_F or V_{FA} as the case may be with $\pi\sqrt{[k_{33}/(\epsilon_o\epsilon_a)]}$ is shown in the inset to Figure 5. Evidently, this equation is only valid[2] for strong anchoring and $\theta_o = 0$; for $\theta_o \neq 0$ or beyond ~80.5 °C, k_{33} so obtained will be generally lower than the actual value, with the deviation becoming ever more marked as θ_o increases.[21b,c] To quantify this error in k_{33}, we determined V_F in the absence of pretilt, for a thick ($d = 68$ μm) sample held between silane treated plates, exhibiting homeotropic alignment through out the nematic range. The corresponding k_{33} values, included in the inset to Figure 5, agree with those for the sample with the anchoring transition to within 5% below ~80.9 °C. For higher temperatures, the difference in k_{33} for the two samples progressively increases as shown in the inset.

D. Destabilization of the Freedericksz State under AC Driving. First we consider the instabilities induced by a 50 Hz field, close to T_{AN}, at ~79.5 °C, for the homeotropic sample with both ϵ_a and σ_a negative. As the voltage is elevated, birefringence color changes due to the dielectric response remain noticeable in the sample till $V \approx 6\ V_F$. It is reasonable to suppose the bulk orientation as uniformly planar at this voltage. Further rise in V destabilizes the homogeneous Freedericksz state at a well-defined threshold, V_o, resulting in the appearance of horizontal stripes between crossed polarizers $P(x)-A(y)$. In Figure 6a presenting the corresponding texture, each stripe has a dark and thin median line with bright bands on either side and, along this line, the director is confined to the xz plane. The periodicity of the stripes along y is far from perfect, with the dark regions between the stripes, where the director stays again confined to the xz plane, possessing varied widths. Seen with diagonal polarizers $P(45)-A(135)$, the dark regions of Figure 6a look pale blue, as in Figure 6b. This corresponds to the sixth order interference color or a path difference of about 2.8 μm which is expected of a 30 μm thick sample with a birefringence of ~0.1 and an almost planar alignment. For parallel polarizers $P(x)-A(x)$, the dark and bright regions of the stripes in Figure 6a show a somewhat reversed contrast, as in Figure 6c. Thus the texture of stripes is more an interference effect than a result of any lens action such as seen in Williams' striations.[1] For the same reason, the stripe-texture practically disappears on using a single polarizer $P(x)$ as evident in Figure 6d.

Characteristically, the stripes which terminate abruptly along x at random, as in Figure 6a, often appear like a string of "beads" or "beans", with their bright bands quasiperiodically fluctuating in intensity along their length (Figure 7). Fragmentation of a stripe into several localized structures, each bilaterally symmetric about x, seems to mark the second stage in the bifurcation sequence at lower frequencies, up to ~75 Hz. The texture of bean-like-objects (BLOs) in Figure 8a is a result of such localization occurring above the threshold. Beyond ~75 Hz, the BLOs appear directly at the primary bifurcation.

The birefringence seen for $P(x)-A(y)$ in the upper and lower halves of each BLO demonstrates the presence of azimuthal tilt of the director in these regions. From a comparison of the birefringence changes that occur in these regions on a slight uncrossing of the analyzer in one sense and then in the other, as illustrated in Figure 8b,c, we may infer the effective azimuthal tilts in the two halves to be opposite in sign and nearly equal in magnitude.

We define the control parameter, ϵ, as usual in nematic electroconvection (NEC), by $\epsilon = (V^2 - V_c^2)/V_c^2$, where V and V_c are respectively the applied and threshold voltages. For the azimuthal instability in Figure 6a, $V_c = V_o = 36.2$ V, at

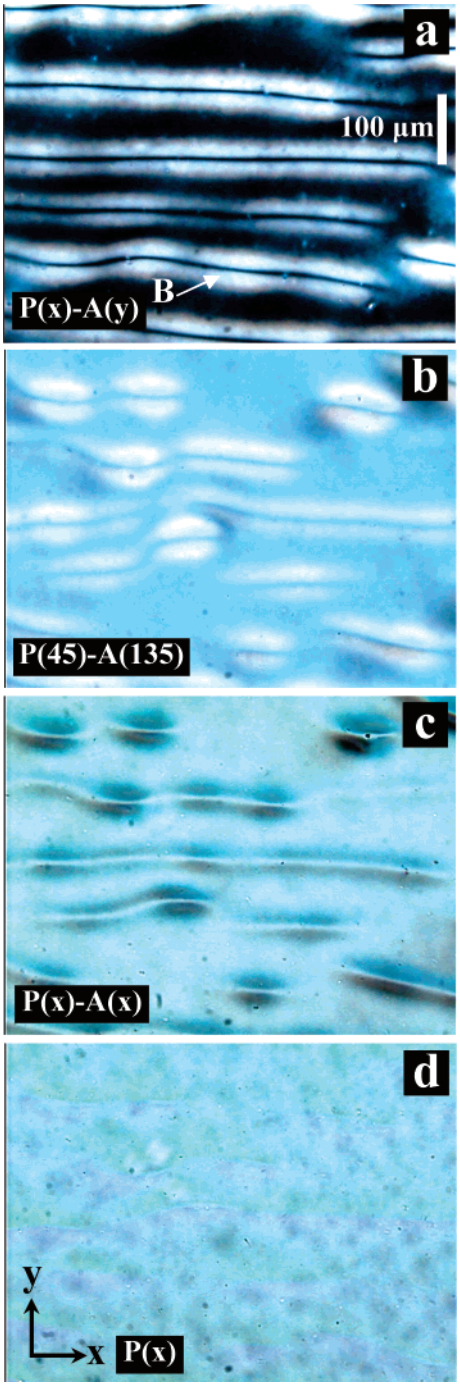

Figure 6. Destabilization of the Freedericksz state by patterned instabilities. 50 Hz, 36.2 V, 79.5 °C. Contrast enhanced reproduction of the textures showing (a) stripes mainly along *x*, each with a median dark line flanked by bright birefringence bands for $P(x)-A(y)$; (b) stripes formed against the sixth order pale blue background as seen between diagonally crossed polarizers; (c) stripes between parallel polarizers showing intensity reversal relative to their texture in panel a; and (d) disappearance of stripes for $P(x)$. Some of the bright bands, such as B in panel a, show a noticeable periodic intensity variation along their length.

79.5 °C. At ϵ slightly above 0, dust particles in the fluid are seen to move along *x*, confined to the median line of the stripes. Quite often this motion stops some way along the line where the particle encounters a structural defect, but when the motion is uninterrupted, it is seen to be oscillatory between the ends of a stripe. The back-and-forth traverse of dust particles, which is more readily observed with the BLOs that form at $\epsilon \approx 0.03$, seems to indicate the stream lines of convective flow to be in

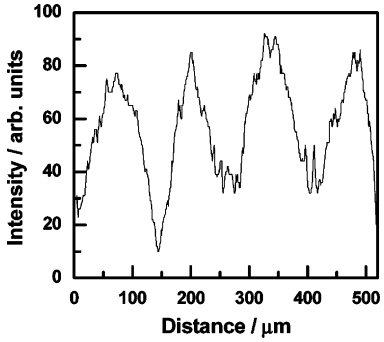

Figure 7. Quasiperiodic intensity variation along the stripe length, ~12 μm below the dark midline of the stripe B in Figure 6a.

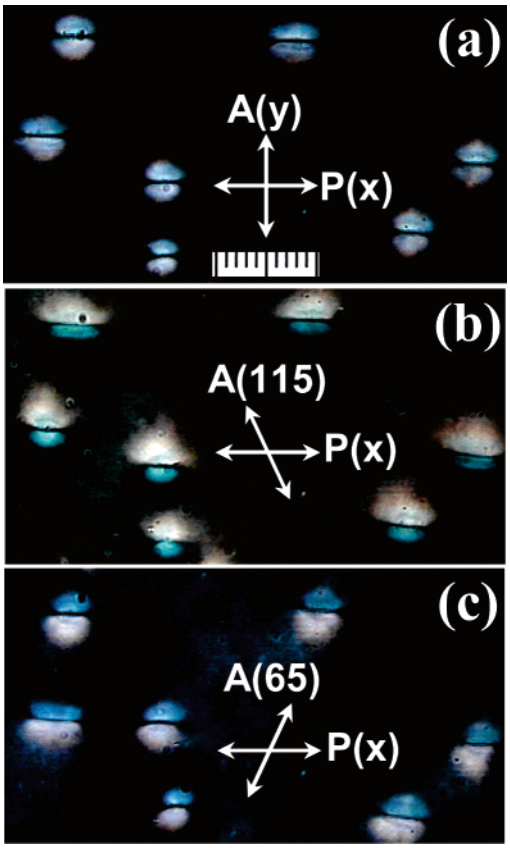

Figure 8. Texture of bean-like objects (BLOs) formed by disintegration of the stripes in Figure 6a, above threshold. 36.9 V, 50 Hz. (a) The upper and lower halves of the BLOs appearing almost with the same pale blue coloration between crossed polarizers. (b) Slight anticlockwise rotation of the analyzer resulting in a difference in color of the two halves and (c) equal rotation of the analyzer in the clockwise sense producing a nearly reverse effect relative to panel b.

the *xz* plane. Conservation of angular momentum further suggests the possibility of a vortex pair associated with each BLO, but this could not be definitively ascertained from the particle motion. The BLOs turn increasingly dynamic as ϵ is further raised and the dust particles in them, which acquire a *y*-component of velocity, appearing to move in a zigzag manner while oscillating along the line of symmetry. At $\epsilon \approx 1.0$, the flows in the BLOs are quasiturbulent; the corresponding texture is illustrated in Figure 9a. At $\epsilon = 1.6$, another bifurcation occurs in the form of horizontal bands periodic in *y* and interrupted by the highly dynamic BLOs, as shown in Figure 9b. This new instability occurs at a characteristic threshold, V_x. Slightly further, at $\epsilon = 1.7$ with reference to V_o, these new bands become more pervasive even as the BLOs turn less turbulent and also

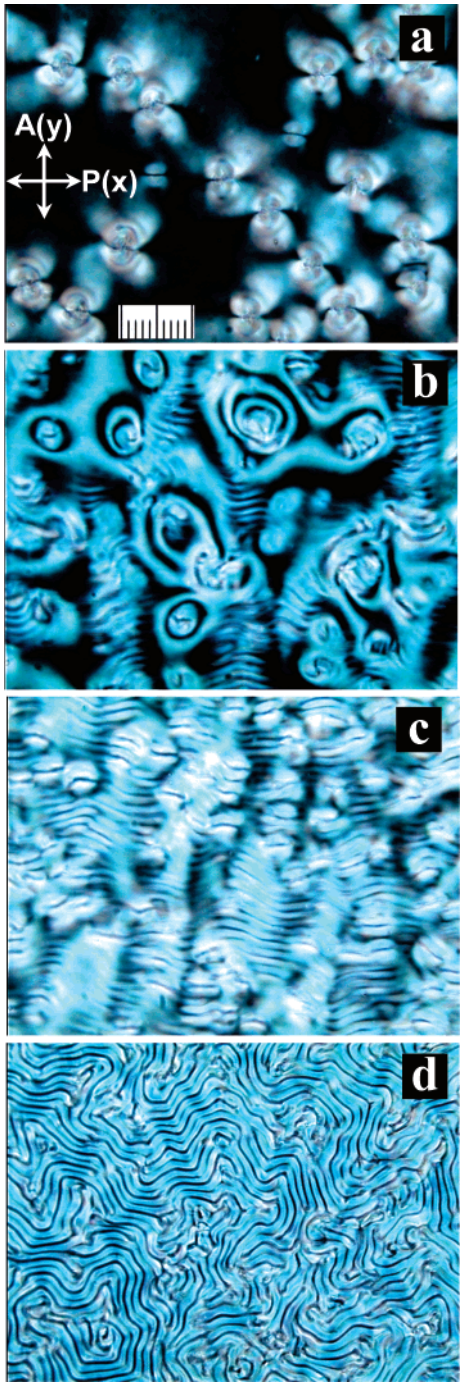

Figure 9. Instabilities far from primary bifurcation under a 50 Hz field for $P(x)-A(y)$. (a) Intense agitation of the fluid in the region of BLOs at 51.3 V. (b) Development of a new azimuthal instability in the form of periodic striations along x in the regions between the BLOs, at 58.6 V. (c) Extensive and slightly undulatory appearance of the azimuthal bands running along x, at 59.6 V. (d) Fingerprint-like texture formed by the azimuthal bands curling around the BLOs, at 69.8 V.

less extensive, as in Figure 9c. Far from equilibrium, at $\epsilon \approx 2.7$, the periodic bands curve around the BLOs to form a fingerprint-like texture as presented in Figure 9d. Further rise in applied bias renders this texture time-varying and at $\epsilon \approx 4.5$, a dynamic scattering like situation is obtained.

Both the thresholds V_o and V_x display a well-marked and similar variation with frequency f, as in Figure 10; further, as depicted in the inset, this variation is linear in $\sqrt{f}$. The threshold periodicity λ_y of the stripes that appear at V_x decreases progressively with rising frequency as in Figure 11; here the

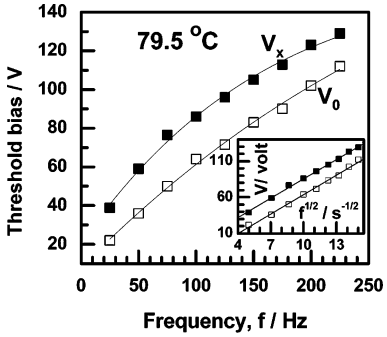

Figure 10. Frequency dependence of the thresholds V_o and V_x for the bifurcations corresponding respectively to a pattern of irregularly spaced x-stripes below ~75 Hz (or bean-like objects above ~75 Hz) and periodic x-stripes. Inset shows the linear variation of both the thresholds with $\sqrt{f}$.

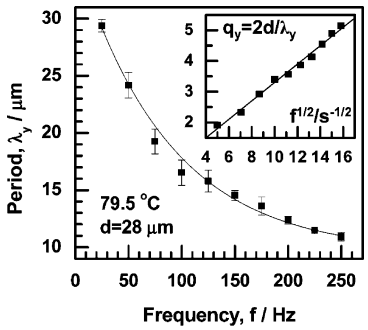

Figure 11. Dependence on frequency of the threshold period λ_y for the x-stripes-instability occurring at V_x. Inset shows the critical wave number q_y varying linearly with $\sqrt{f}$.

inset shows the linear dependence of the corresponding critical wave vector on $\sqrt{f}$.

We may now consider the sequence of instabilities above the conductivity isotropy point, at 82 °C, where $\sigma_a > 0$ while ϵ_a remains negative. Figure 12 presents what we may call the "cowry-shell (CS)" texture corresponding to the primary bifurcation occurring at the threshold bias V_y and frequency of 25 Hz. The CSs are indeed the BLOs with a superimposed pattern of close-spaced focal images along the midline. Clearly, the CS structure is composed of both polar and azimuthal director deviations, the former that causes refractive index modulation for the extraordinary vibration along x as in Williams' domains, evident in Figures 12a and 12b and the latter emphatically manifesting in Figure 12c. The focal images in Figure 12a may be looked upon as stripes parallel to and strongly localized along y. In fact, on progressively increasing the bias above V_y, these stripes become evermore extensive spatially, as in Figure 13a−d. Simultaneously, the BLOs turn increasingly dynamic. At $V \approx 1.8\ V_y$, the stripes become oblique, forming a chevron-type texture (Figure 14). Far above the threshold, at $\sim 6.5 V_y$, the pattern becomes time dependent as in the dynamic scattering case.

The threshold V_y scales linearly with $\sqrt{f}$ (Figure 15), just as the thresholds V_o and V_x. The CS instability occurs only for frequencies up to ~75 Hz beyond which the stripes form directly within randomly localized domains; these domains enlarge with increasing voltage. The critical periodicity λ_x and the corresponding wave vector vary with f as illustrated in Figure 16.

E. Effect of a Static Field. Under dc driving, as expected, the Freedericksz transition takes place just as under ac driving for both (− − h) and (− + t) configurations. Intriguingly, however, no electroconvective bifurcations are observed above V_F in either case. This has been verified by raising the field up

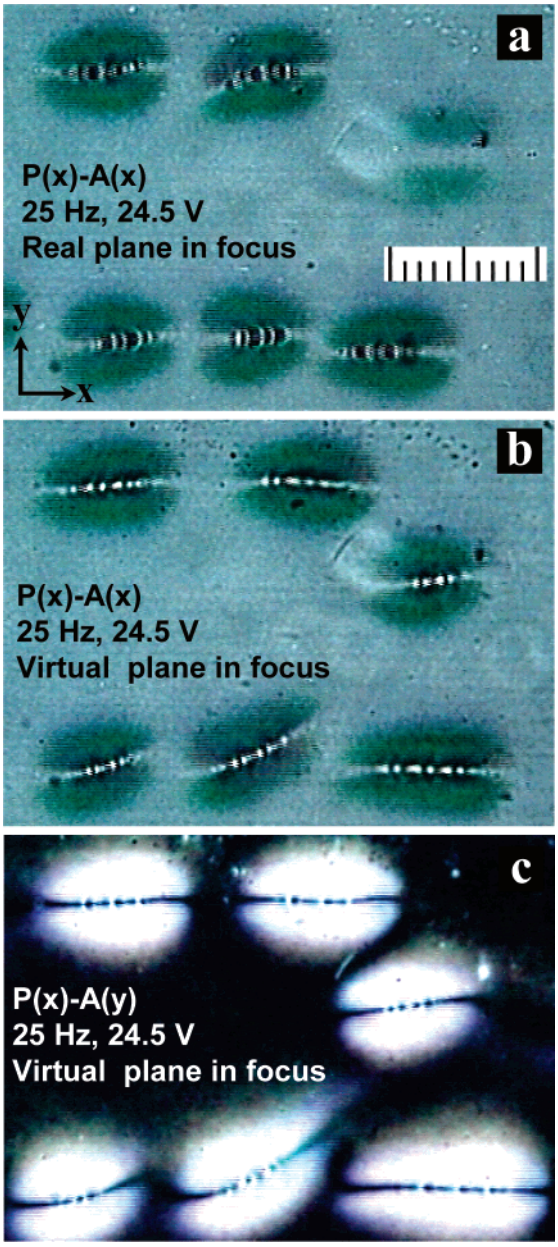

Figure 12. Hybrid textures due to interplay between the bean and stripes instabilities, observed at 82 °C. Quasi-periodic striations along the midline of BLOs in their (a) real focal plane and (b) virtual focal plane, with the focusing action involving periodic director deviations in the *xz* plane. (c) The strong azimuthal tilt of the director in the upper and lower halves of the beans revealing between crossed polarizers.

to the sample break down (~150 V). By comparison, even at very low frequencies (<1 Hz) of ac fields, the convective instabilities occur. That this effect relies on field gradients becomes evident from a low-frequency square wave excitation; then the patterned states develop only during the polarity reversals and disappear after the field attains a constant value. This result is obviously of relevance in understanding the mechanism responsible for the patterned states.

Significance of the Patterned States

An intriguing aspect of the patterned instabilities described in the previous sections is their occurrence exclusively in ac fields. At high voltages, the reduction of the bulk field due to the double layers forming at the electrodes would seem to be negligible and, in any case, the dielectric response occurs at a much lower voltage. Thus we are led to the conclusion that flexoelectric distortions generated by the field gradients present during polarity switch over play a crucial role in the establishment of patterned states.

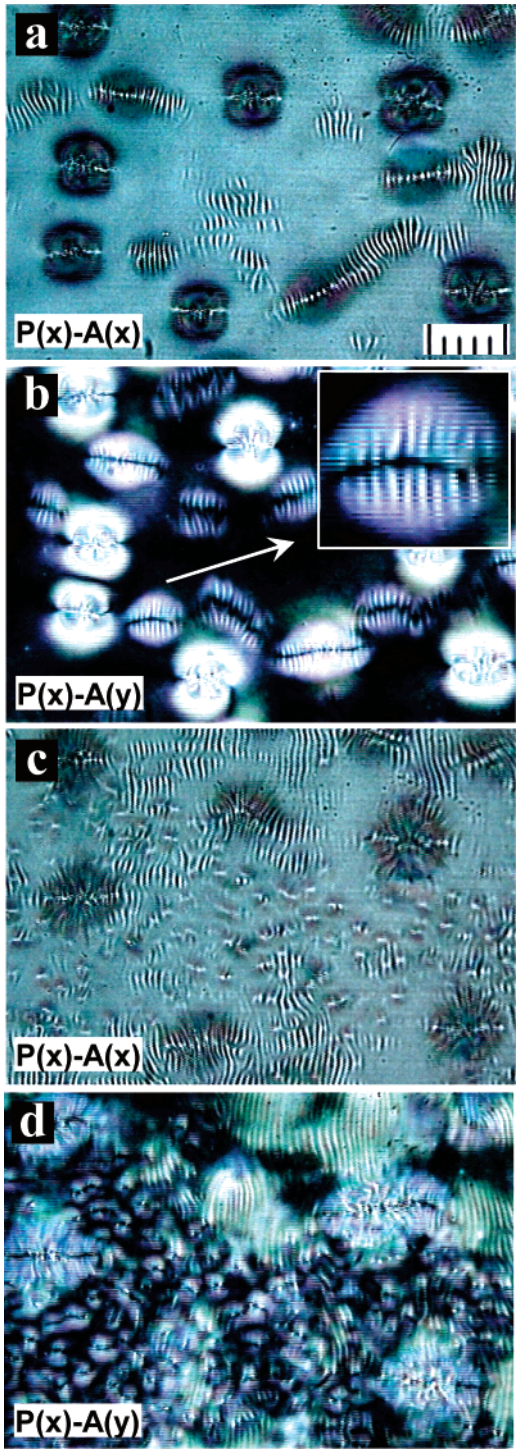

Figure 13. Dominance of the *y*-stripes instability due to a 25 Hz field, well above the threshold V_y at 82 °C. (a, b) 29.8 V; (c, d) 34 V.

The texture of BLOs such as in Figure 8a has previously been reported for a (+ + p) nematic and attributed to the destabilization of the Freedericksz state by the isotropic mode of electroconvection that originates from a nonuniform distribution of charges along the field direction.[22] Significantly, in this case, the fluid circulations are noted to be around the BLOs in the *xy* plane, occurring in the two boundary layers in a correlated manner, with the sense of rotation reversing between the upper

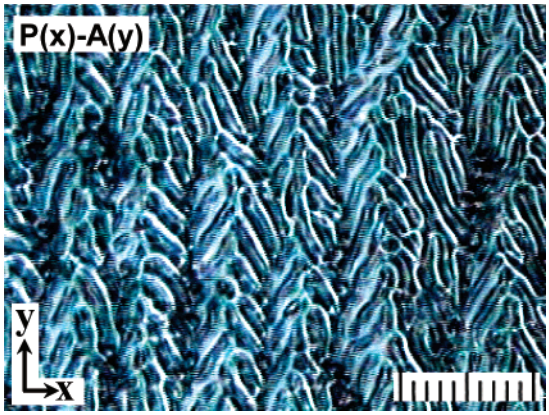

Figure 14. Texture of chevrons into which the *y*-stripes transform with the rise in voltage amplitude. The contrast difference between the stripes with opposite inclinations reflects the correspondingly opposite azimuthal deviations. 25 Hz. 41.3 V.

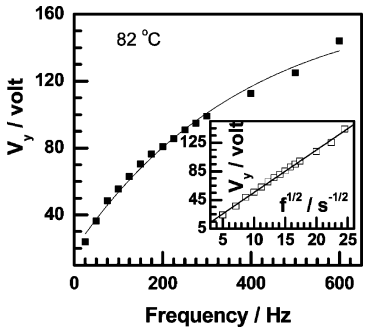

Figure 15. Frequency dependence of the threshold V_y corresponding to the periodic y-striation instability. Inset shows the linear variation of the threshold with $\sqrt{f}$.

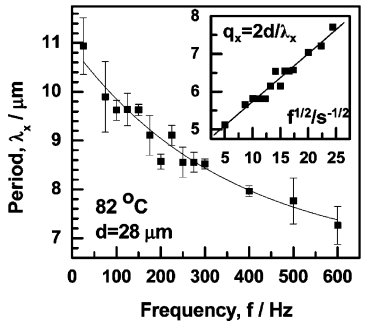

Figure 16. Dependence on frequency of the threshold period λ_x for the *y*-stripes instability occurring at V_y. Inset shows the critical wave number q_x varying linearly with $\sqrt{f}$.

and lower vortices around a common axis. In **10**/**5**, we could not detect such pairs of vortices, but the chance particles trapped in the BLOs seemed to oscillate along the midline, as earlier mentioned. However, spatial charge inhomogeneities may be involved in the formation of BLOs particularly in view of the need for ac fields to produce them.

Localized time-dependent states have also been observed in nematic 4′-hexyloxyphenyl 4-decyloxybenzoate, **10**/**6**;[23] they manifest as anisotropic clusters of short oblique rolls at low frequencies and flickering butterfly-like objects resembling the BLOs at high frequencies; these instabilities occur in the vicinity of the smectic−nematic transition temperature where σ_a turns negative and $\epsilon_a < \sigma_a < 0$; in this situation, since the Carr−Helfrich mechanism breaks down, these localized states do not conform to the standard model.

Regarding the periodic pattern of "*x*-stripes" forming at the threshold V_x, it is similar in some of its characteristics to that of the so-called azimuthal electrohydrodynamic (AEHD) instability,[12,24−26] predicted and observed very early in tilted nematics with the initial director defined by $\mathbf{n} = (\sin\theta, 0, \cos\theta)$; it is related to conical director rotations about either the *x* or the *z*-axis which involve a periodic change along *y* of the azimuthal angle φ between the **c**-director and *x*-axis. In the time dependent model of AEHD, the threshold features are arrived at from an analysis similar to that for the chevron or dielectric regime and it is shown that both V_x and q_y should vary as $\sqrt{f}$. As the insets to Figures 10 and 11 show, these predictions hold good for the *x*-stripes. However, the theory predicts a finite dc threshold for $\theta \neq 90$, which is not observed. More importantly we note that the nematic director well above the bend Freedericksz transition will not be uniformly tilted across the sample thickness as assumed in the theory, but will almost be planar in the bulk. Thus it is natural to consider if electroconvection could set in as a secondary instability driven by the usual CH mechanism applicable to planar samples. In eq 1, since (α_2/η_1) is expected to be of the order of -0.75,[4] using the measured permittivity and conductivity values in Figures 1 and 2, we find $(\zeta^2 - 1)$ to be ~ -3 which precludes the CH instability. Even according to the SM, this instability is excluded in the $(- - p)$ case.[15−18] Interestingly, as shown by Madhusudana and Raghunathan,[27a] when flexoelectric terms are incorporated into the one-dimensional CH theory for the $(- - p)$ case, electroconvection becomes possible. Significantly, the theoretical-numerical analysis in ref 27a for certain chosen values of material parameters, while providing no solution corresponding to the conduction regime, shows the existence of a nearly longitudinal roll instability in the dielectric regime characterized by the field threshold and $q_y \approx \pi/d$; however, it does not provide any solution for the frequency regime where $q_y \gg \pi/d$. It is necessary to note, when the flexoeffect becomes important or the lowest order time-Fourier approximation employed in the generalized CH theory breaks down,[27b] the sharp distinction between conduction and dielectric instabilities no longer exists.

Coming to the pattern of "*y*-stripes" as in Figure 13, they are, over a wide frequency range, too closely spaced to be regarded as corresponding to conventional normal rolls (NR).[3] Moreover, we could detect no regular cellular flows associated with the pattern of *y*-stripes, unlike in the NR pattern, although time-dependence of the pattern occurred at higher voltages. On the other hand, the $\sqrt{f}$ dependence of V_y and q_x as seen in the insets to Figures 15 and 16, as well as the chevron texture in Figure 14, are among the distinguishing features of the instabilities that usually belong to the dielectric regime in planar samples.[4] This is not surprising when we consider the low cutoff frequency f_c expected for the conduction regime. For example, with 0.75 for $(-\alpha_2/\eta_1)$ as in MBBA,[4] using the ϵ and σ data from Figures 1 and 2, we find f_c to be about 16 Hz. Again we note, the formation of striped state only during polarity changes under low-frequency square wave driving renders any analysis that does not consider the field gradients less meaningful and consideration of flexoeffect implies coupling of the conduction and dielectric modes.

Conclusions

We have demonstrated the formation of an ordered sequence of patterned states within the dielectrically reoriented $(- - h)$ and $(- + t)$ samples of **10**/**5**. In the $(- - h)$ case, the patterns, all of which involve azimuthal director-deviations, occur with increasing control parameter in the order (i) broad, irregularly spaced, parallel-to-*x*-stripes, (ii) localized bean-like domains derived from the broad stripes, (iii) quasiturbulent localized

domains, (iv) narrow-spaced *x*-stripes with well-defined wave number q_y, and (v) fingerprint texture. In (− + t) samples, the pattern order is (i) hybrid localized azimuthal instability with superimposed parallel-to-*y* stripes, (ii) extended *y*-stripe-domains and (iii) chevron instability. We cannot describe any of these instabilities as "standard" in the sense of the Carr−Helfrich mechanism based standard model.[16] However, the extended 1-D CH theory[27a] that includes the flexoelectric terms explains some of the observed features like the *x*-stripes with $q_y \approx \pi/d$ and the frequency variation of their threshold. The absence of convection under dc excitation points to the particular importance of gradient flexoeffect in causing patterned states under charge injection conditions. These results point to the need for generalizing the SM for ac fields by considering flexoeffects and also considering hybrid instabilities due to the coupling between CH and isotropic convections.

Acknowledgment. We thank Professor K. A. Suresh for his keen interest in this investigation, Dr. S. Krishna Prasad and Professor W. Weissflog for the liquid crystal samples, and Dr. Agnes Buka for useful suggestions on the manuscript.

References and Notes

(1) Blinov, L. M.; Chigrinov, V. G. *Electrooptic Effects in Liquid Crystal Materials*; Springer: Berlin, 1994.

(2) Pikin, S. A. *Structural Transformations in Liquid Crystals*; Gordon and Breach Science Publishers: New York, 1991.

(3) Kramer, L. In *Pattern Formation in Liquid Crystals*; Buka, A., Kramer, L., Eds.; Springer: Berlin, 1996.

(4) De Gennes, P. G.; Prost, J. *The Physics of Liquid Crystals*; Clarendon Press: Oxford, 1993.

(5) Delev, V. A.; Krekhov, A. P.; Kramer, L. *Mol. Cryst. Liq. Cryst*. **2001**, *366*, 849.

(6) Dressel, B.; Joets, A.; Pastur, L.; Pesch, W.; Plaut, E.; Ribotta, R. *Phys. Rev. Lett.* **2002**, *88*, 24503.

(7) Dressel, B.; Pesch, W. *Phys. Rev. E* **2003**, *67*, 31707.

(8) Pramoda Kumar; Krishnamurthy, K. S. *Phys. Rev. E* **2006**, *74*, 031705.

(9) Ribotta, R. In *Solitons in Liquid Crystals*; Lam, L., Prost, J., Eds.; Springer: Berlin, 1992.

(10) Dubois-Violette, E.; de Gennes, P. G.; Parodi, O. *J. Phys. (Paris*) **1971**, *32*, 305.

(11) (a) Goscianski, M. *Philips Res. Repts*. **1975**, *30*, 37. (b) Goscianski, M.; Leger, L. *J. Phys. (Paris*) **1975**, *36*, C1−231.

(12) Tikhomirova, N. A.; Ginzberg, A. V.; Kirsanov, E. A.; Bobyshev, Yu. P.; Pikin, S. A.; Adomenas, P. V. *JETP Lett*. **1977**, *24*, 269.

(13) Blinov, L. M.; Barnik, M. I.; Lazareva, V. T.; Trufanov, A. N. *J. Phys. (Paris*) **1979**, *40*, C3−263.

(14) Petrov, M.; Simova, P. In *Forschungen über Flüssige Kristalle*; Demus, D., Ed.; Martin-Luther-Universatät Halle-Winttenberg: Halle, Germany, 1983.

(15) Kochowska, E.; Nemeth, S.; Pelzl, G.; Buka, A. *Phys. Rev. E* **2004**, *70*, 011711.

(16) Bodenschatz, E.; Zimmermann, W.; Kramer, L. *J. Phys. (Paris)* **1988**, *49*, 1875.

(17) Toth-Katona, T.; Cauquil-Vergnes, A.; Eber, N.; Buka, A. *Phys. Rev. E* **2007**, *75*, 66210.

(18) Buka, A.; Eber, N.; Pesch, W.; Kramer, L. In *Self-Assembly, Pattern Formation and Growth Phenomena in Nanosystems*; Golvin, A., Ed.; Kluwer Academic Press: New York, 2005.

(19) Kresse, H.; Wiegeleben, A.; Demus, D. *Krist. Tech*. **1980**, *15*, 341.

(20) (a) Shioda, T.; Wen, B.; Rosenblatt, C. *Phys. Rev. E* **2003**, *67*, 041706−1. (b) Känel, H. V.; Litster, J. D.; Melngailis, J.; Smith, H. I. *Phys. Rev. A* **1981**, *24*, 2713.

(21) (a) Yang, D.-K.; Wu, S.-T. *Fundamentals of Liquid Crystal Devices*; Wiley: Chichester, U.K., 2006. (b) Rapini, A.; Papoular, M. *J. Phys. (Paris)* **1969**, *30*, C4−54. (c) Chigrinov, V. G.; Grebenkin, M. F. *Kristallografiya* **1975**, *20*, 1240.

(22) (a) Blinov, L. M.; Trufanov, A. N.; Chigrinov, V. G.; Barnik, M. I. *Mol. Cryst. Liq. Cryst*. **1981**, *74*, 1. (b) Trufanov, A. N.; Barnik, M. I.; Blinov, L. M.; Chigrinov, V. G. *Sov. Phys. JETP* **1981**, *53*, 355.

(23) Brand, H. R.; Fradin, C.; Finn, P. L.; Pesch, W.; Cladis, P. E. *Phys. Lett. A* **1998**, *235*, 508.

(24) Pikin, S. A.; Chigrinov, V. G.; Indenbom, V. L. *Mol. Cryst. Liq. Cryst*. **1976**, *37*, 313.

(25) Pikin, S. A.; Indenbom, V. L. *Sov. Phys. Crystallogr*. **1975**, *20*, 1127.

(26) Pikin, S.; Ryschenkow, G.; Urbach, W. *J. Phys. (Paris)* **1976**, *37*, 241.

(27) (a) Madhusudana, N. V.; Raghunathan, V. A. *Liq. Cryst*. **1989**, *5*, 1789. (b) Thom, W.; Zimmermann, W.; Kramer, L. *Liq. Cryst*. **1989**, *4*, 309.